Supplementary Materials for

Surface charge transfer doping of narrow-bandgap Sn-Pb perovskites toward high performance tandem solar cells

Qiang Sun[a], Zhiguo Zhang[a], Haixuan Yu[a], Junyi Huang[a], Xiongjie Li[a], Letian Dai[a], Qi Wang[b], Yan Shen*[a], Mingkui Wang*[a,c]

[a] Wuhan National Laboratory for Optoelectronics, Huazhong University of Science and Technology, 1037 Luoyu Road, Wuhan 430074, Hubei, P. R. China. E-mail: ciac_sheny@hust.edu.cn, mingkui.wang@hust.edu.cn

[b] CSG HOLDING CO., LTD. CSG Building, No.1, Industrial 6th road, Mechants Street, Nanshan District, Shenzhen, P.R. China

[c] Optics Valley Laboratory, Wuhan, Hubei 430074, P.R. China

Materials.

FAI (99.9%, Xi'an Polymer), MAI (99.9%, Xi'an Polymer), CsI (99.9%, Sigma Aldrich), PbI_2 (99.999%, Alfa Aesar), SnI_2 (99.99%, Sigma Aldrich), SnF_2 (99%, Sigma Aldrich), $PbBr_2$ (99.99%, Sigma Aldrich), Tin powders (99%, Sigma Aldrich), *N, N*-Dimethylformamide (DMF, Anhydrous 99.8%, Sigma Aldrich), dimethyl sulfoxide (DMSO, Anhydrous 99.5%, Sigma Aldrich), Chlorobenzene (CB, Anhydrous 99.8%, Sigma Aldrich), PTAA (99.8%, Xi'an Polymer), PEDOT:PSS (4083, Xi'an Polymer), C_{60} (99%, Nano-C), BCP (99.99%, Sigma Aldrich), benzyl viologen dichloride (97%, Sigma Aldrich) were used as received.

Benzyl Viologen Preparation:

The BV solution was prepared according to previous reports.[1, 2] Firstly, 700 mg of benzyl viologen dichloride was dissolved in 20 mL deionized water, then 10 mL Toluene was carefully added on the deionized water to form a bilayer system. After that, 400 mg of $NaBH_4$ was added to the reaction system which induces the two-electron reduction of the viologen salt. The reaction was performed under constant nitrogen bubbling for 60 minutes. The BV layer in toluene was then drawn into a syringe and transferred to a sealed vial for further use.

Perovskite films preparation.

The perovskite precursor solutions were prepared in argon filled glovebox with $H_2O<0.1$ ppm and $O_2<0.5$ ppm. FAI, MAI, PbI_2, SnI_2, SnF_2 with molar ratio of 1.4:0.6:1:1:0.1 were dissolved in mixed solvent of DMF and DMSO (v/v, 4:1) to form 1.8 M $FA_{0.7}MA_{0.3}Pb_{0.5}Sn_{0.5}I_3$ precursor solution. To reduce Sn^{4+} in the precursor solution, tin powders (10 mg mL^{-1}) were added and stirred at room temperature for 60 min, the remaining tin powders were filtered with 0.22 μm PTFE membrane. CsI, FAI, PbI_2, $PbBr_2$ with molar ratio of 0.2:0.8:0.4:0.6 were dissolved in mixed solvent of DMF and DMSO (v/v, 4:1) to form 1.1 M $Cs_{0.2}FA_{0.8}PbI_{1.8}Br_{1.2}$ precursor solution. All perovskite precursor solutions were prepared 3 hours before perovskite films deposition. For narrow bandgap $FA_{0.7}MA_{0.3}Pb_{0.5}Sn_{0.5}I_3$ films, the precursor solution was deposited through a one-step spin-coating process (1500 rpm for 10 s and 5000 rpm for 30 s) with dripping of CB as anti-solvent at 10-12 s before the end. Subsequently, the spin-coated perovskite films were thermally annealed at 50 °C for 1 min and 120 °C for 10 min. For wide bandgap $Cs_{0.2}FA_{0.8}PbI_{1.8}Br_{1.2}$ films, the precursor solution was deposited through a one-step spin-coating process (5000 rpm for 30 s)

with dripping of CB as anti-solvent at 13-15 s before the end. Subsequently, the spin-coated perovskite films were thermally annealed at 50 °C for 1 min and 150 °C for 30 min.

Narrow bandgap $FA_{0.7}MA_{0.3}Pb_{0.5}Sn_{0.5}I_3$ PSC Fabrication.

For narrow bandgap $FA_{0.7}MA_{0.3}Pb_{0.5}Sn_{0.5}I_3$ PSCs. PEDOT: PSS films were coated on the cleaned ITO-glasses at 4500 rpm for 40 s and then annealed in air at 145 °C for 20 min. The narrow bandgap $FA_{0.7}MA_{0.3}Pb_{0.5}Sn_{0.5}I_3$ films were deposited onto ITO/PEDOT: PSS substrates as described above. Finally, C60 (20 nm), BCP (6 nm) and Ag (100 nm) were subsequently deposited onto the perovskite films by thermal evaporation. The active area of the devices was 0.06 cm^2 defined by a shadow mask.

Monolithic 2T all-perovskite tandem solar cell fabrication.

2T all-perovskite tandem solar cells were built by stacking narrow-bandgap subcells on top of wide-bandgap subcells. Top wide-bandgap subcells were first fabricated. PTAA (2mg mL^{-1} in chlorobenzene) were deposited onto ITO substrates as the hole transport layer. The $Cs_{0.2}FA_{0.8}PbI_{1.8}Br_{1.2}$ perovskite films were deposited onto ITO/PTAA substrates as described above. C60 (20 nm) was subsequently deposited onto the perovskite films by thermal evaporation. In the following, 24 nm of SnO$_x$ layer was deposited by atomic layer deposition at 100 °C from 200 cycles of tetrakis(dimethylamino)tin (IV) (TDMASn; Aimouyuan) and deionized water. Then, the samples were transferred to a thermal evaporator to deposit 1-nm-thick Au interconnecting layer. In the end, the devices followed the same fabrication process of narrow-bandgap $FA_{0.7}MA_{0.3}Pb_{0.5}Sn_{0.5}I_3$ PSC to complete the construction of 2T tandem solar cells.

Characterization.

X-ray diffraction (XRD) were conducted using a Philips X-ray diffractometer with Cu Kα radiation. UV-visible absorption spectra were observed with PerkinElmer LAMBDA 950 spectrophotometer. XPS measurements were performed on a Kratos AXIS Ultra-DLD ultra-high-vacuum photoemission spectroscopy system. Top view and cross section SEM images of the samples were obtained with FEI Nova NanoSEM 450. Time-resolved photoluminescence decay measurements were performed with a 478 nm light pulse as excitation by Delta Flex Fluorescence Lifetime System (Horiba Scientific Com., Japan). Hall-effect measurements were conducted using ECOPIA

HMS-5500 Hall-effect measurement system with 4-contact van der Pauw method in ambient air. The Sn-Pb perovskite films were encapsulated with cover glass using UV-adhesive, and the Ag contacts outside the encapsulation area were connected to the controller for Hall-effect measurement. KPFM was measured by Kevin probe force microscopy (KPFM, Bruker dimension icon) in argon filled glove box at room temperature. The samples were glue to the sample stage by conductive silver paste. The surface potential distribution of the samples was collected in AM-KPFM mode by a conductive Pt/Ir coated probes (tip model: SCM-PIT with k=0.28 N/m, Bruker Corporation). Image scan rate was set to be 1 Hz per line with a resolution of 256×256 pixels. The lift height was set to be 100 nm. PLQY measurements were conducted using Quanta Master 8000 (HORIBA). The samples were excited with a 520 nm laser beam. The intensity of the laser was adjusted to 1-sun equivalent intensity by illuminating a perovskite solar cell under short-circuit and matching the current density to the J_{SC} measured under the sun simulator. A second optical fiber was used from the output of the integrating sphere to an Andor SR393iB spectrometer equipped with a silicon CCD camera (DU420A-BR-DD, iDus). The system was calibrated by using a calibrated halogen lamp with specified spectral irradiance, which was shone into to integrating sphere. A spectral correction factor was established to match the spectral output of the detector to the calibrated spectral irradiance of the lamp. The spectral photon density was obtained from the corrected detector signal (spectral irradiance) by division through the photon energy (hf), and the photon numbers of the excitation and emission obtained from numerical integration using Matlab. In a last step, three fluorescent test samples with high specified PLQY (~70%) supplied from Hamamatsu Photonics where measured where the specified value could be accurately reproduced within a small relative error of less than 5%. The impedance spectroscopy for DOS analysis were performed using the PGSTAT302N frequency analyzer (Autolab, the Netherlands) together with the Frequency Response Analyzer to give voltage modulation under the giving range of frequency. The electronic impedance spectra of the devices were recorded at potentials varying from -1.0 V to 0 V at frequencies ranging from 10 Hz to 1 MHz, the oscillation potential amplitudes being adjusted to 10 mV. The Z-view software was use to analyze the impedance data to get the chemical capacitance values for DOS analysis. A xenon light source solar simulator (450 W, Oriel, model 9119) with an AM 1.5 G filter (Oriel, model 91192) was used to give an irradiance of 100 mWcm^{-2} at the surface of the solar cells. The photocurrent density-voltage (*J-V*) characteristics of the perovskite solar cell devices were measured by recording the current through Keithley 2400

digital source meter. A similar data acquisition system was used to control the incident photon-tocurrent conversion efficiency (EQE) measurement.

DFT calculations.

The first principles computations were carried out by Vienna Ab initio Simulation Package (VASP) based on density functional theory. Generalized gradient approximation (GGA) with the Perdew-Burke-Ernzerhof (PBE) functional was used to describe the exchange-correlation interaction. The projector augmented wave pseudopotentials were adopted to describe the ion-electron with a cutoff energy of 500 eV. The K-point grid of Brillouin zone was tested and sampled by 3×3×1 within Gamma-Pack. The electronic energy and forces were converged to within 10^{-5} eV and 0.03 eVÅ^{-1}, respectively. The vacuum layer in the slab model is larger than 15 Å to avoid superficial interaction between periodical slabs. In order to calculate the binding energy of BV molecule on Sn-Pb perovskite surface, the following expression was used: $E_{\text{binding}} = E_{\text{surf+BV}} - E_{\text{surf}} - E_{\text{BV}}$, where $E_{\text{surf+BV}}$, E_{surf}, and E_{BV} are the total energies of the surface with BV molecule, the clean surface, and the BV molecule, respectively.
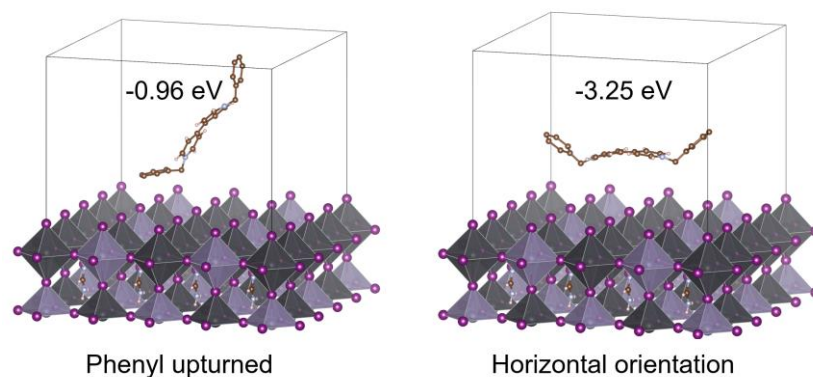
Figure S1. Schematic illustration and the calculated binding energy of two possible orientations (phenyl upturned, and whole molecule horizontal orientation) of BV on Sn-Pb perovskite surface.

The mechanism how BV is attached to the Sn-Pb perovskite surface is revealed by additional density functional theory (DFT) calculations. As shown in Figure S1, we systematically modeled two possible orientations (one for phenyl upturned, and another for the whole molecule horizontal orientation) of the absorbent BV onto the Sn-Pb perovskite surface. The binding energy for the BV horizontal orientation exhibits a significant high absolute value (−3.25 eV) compare to that (−0.96 eV) of the phenyl upturned case, indicating that the BV molecules preferentially exhibit a horizontal orientation on the Sn-Pb perovskite surface.
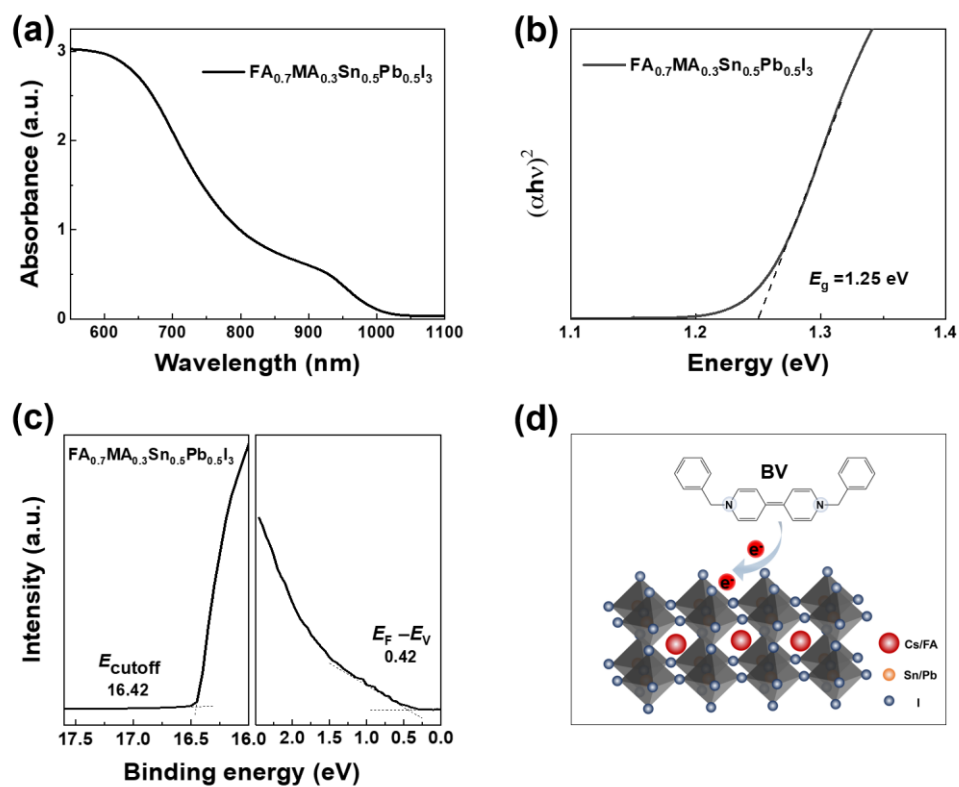
Figure S2. The (a) UV-vis absorption spectra and (b) the Tauc's plots of $FA_{0.7}MA_{0.3}Sn_{0.5}Pb_{0.5}I_3$ perovskite film; (c) The ultraviolet photoelectron spectroscopy of $FA_{0.7}MA_{0.3}Sn_{0.5}Pb_{0.5}I_3$ perovskite; (d) Schematic diagram of surface charge transfer doping compensation of the narrow-bandgap Sn-Pb binary metal perovskite by BV molecule.
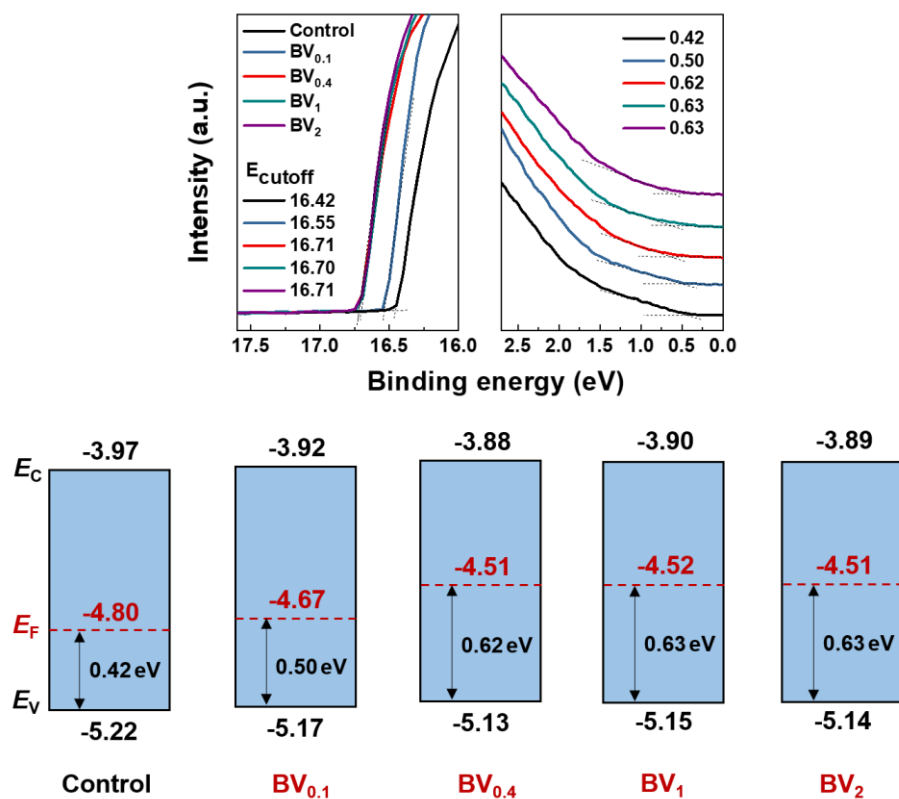
Figure S3. The energy level diagram of the Sn-Pb perovskite films various BV concentrations (0, 0.1, 0.4, 1 and 2 mgL^{-1}) obtained from UPS measurements.
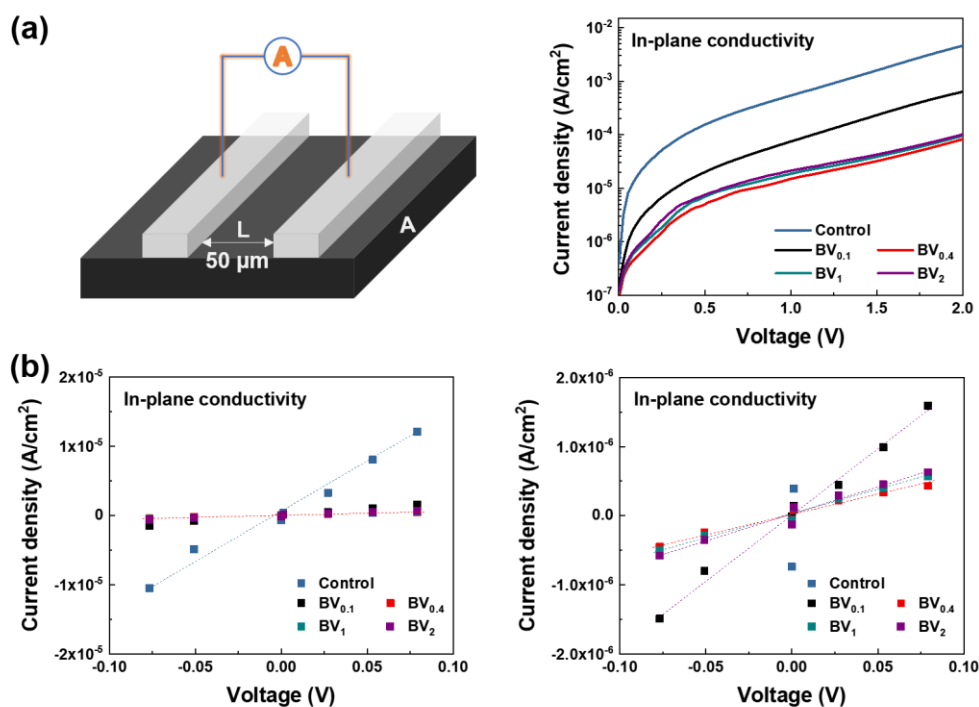
**Figure S4**. (a) The in-plane electrical conductivity of the Sn-Pb perovskite films with various BV concentrations (0, 0.1, 0.4, 1 and 2 mgL^{-1}) measured by scanning the current density-voltage curves in the gap-type structure. (b) The in-plane conductivity value determined by fitting the slope of the current density-voltage curves near 0 V.

The in-plane conductivity (σ) was measured by scanning the current density-voltage curves of the Sn-Pb perovskite films with a gap-type structure using a Keithley 2400 digital source meter in argon filled glovebox (Figure S3a). The in-plane conductivity (σ) value was determined by fitting the slope of the current density-voltage curves near 0 V (Figure S3b), and can be calculated based on the equation $\sigma = L/(R \cdot A)$, where R is the resistance, A is the area of the cross and L is width of the channel.[3-5] The in-plane conductivity (σ) value of the control and the BV treated Sn-Pb perovskite films are calculated to be 5.75×10^{-5} S m^{-1} (control), 8.24×10^{-6} S m^{-1} (BV$_{0.1}$), 2.26×10^{-6} S m^{-1} (BV$_{0.4}$), 2.74×10^{-6} S m^{-1} (BV$_{1}$), 3.12×10^{-6} S m^{-1} (BV$_{2}$), respectively.
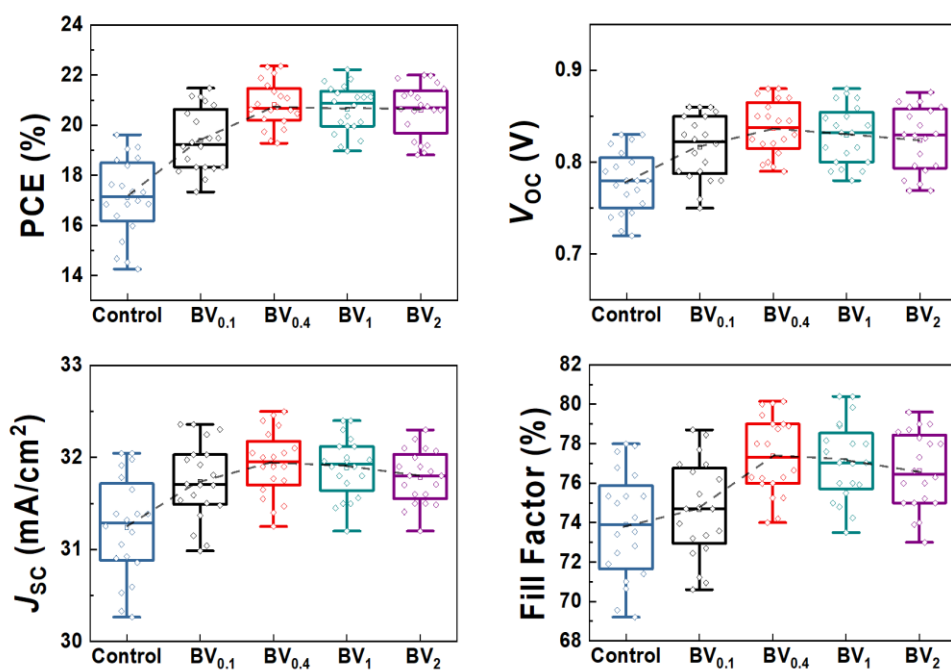
Figure S5. The statistic PV parameters of the PSCs (20 devices per type) with various BV concentrations (0, 0.1, 0.4, 1 and 2 mgL^{-1}).
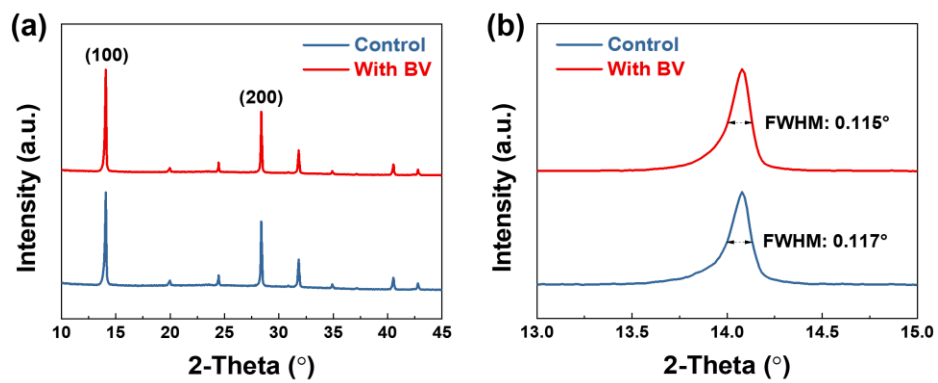
Figure S6. The XRD patterns of the control and BV-treated Sn-Pb perovskite films.
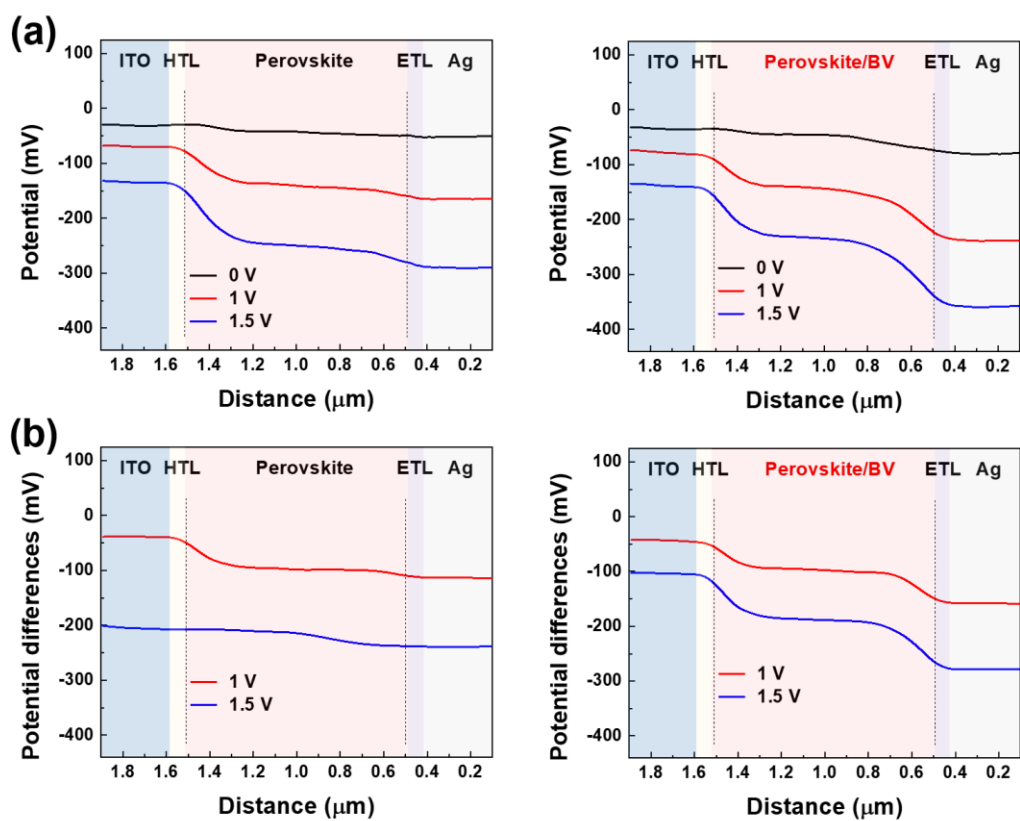
Figure S7. The averaged potential line profiles obtained from Kelvin probe force microscopy measurements and the potential differences with respect to the zero bias of the PSCs with or without BV incorporation.
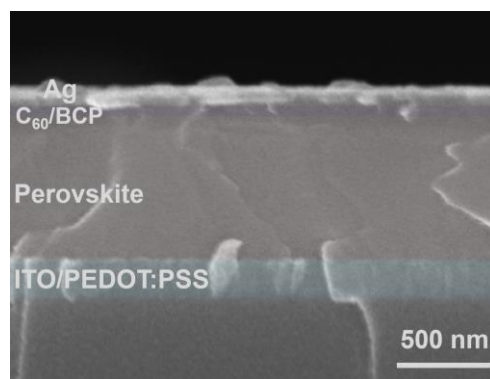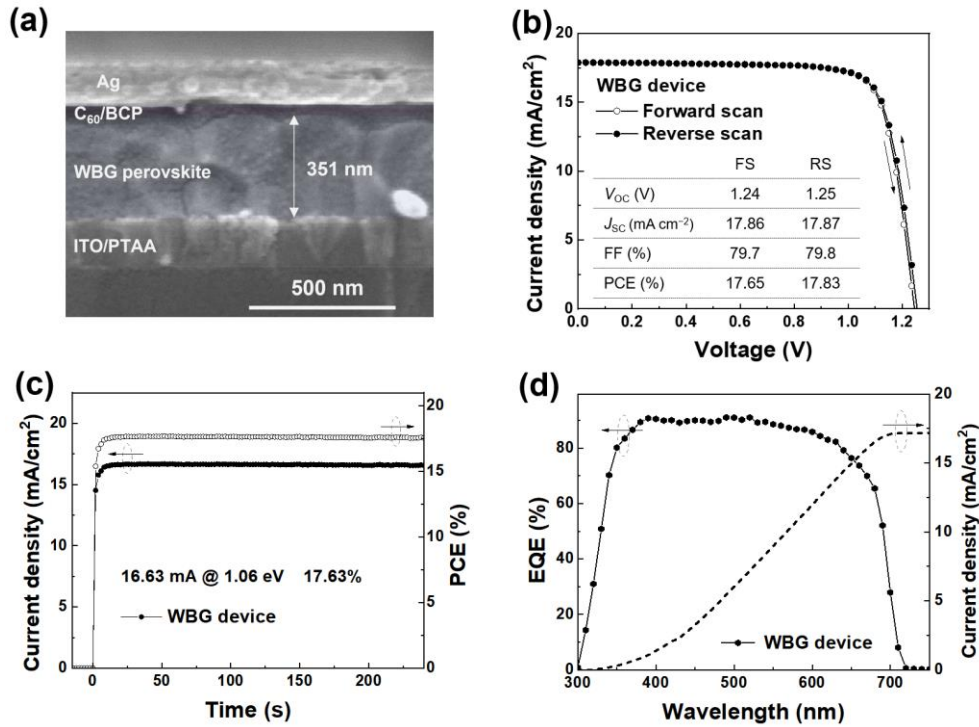
Figure S8. Cross-sectional SEM image of the narrow-bandgap $FA_{0.7}MA_{0.3}Sn_{0.5}Pb_{0.5}I_3$ device.
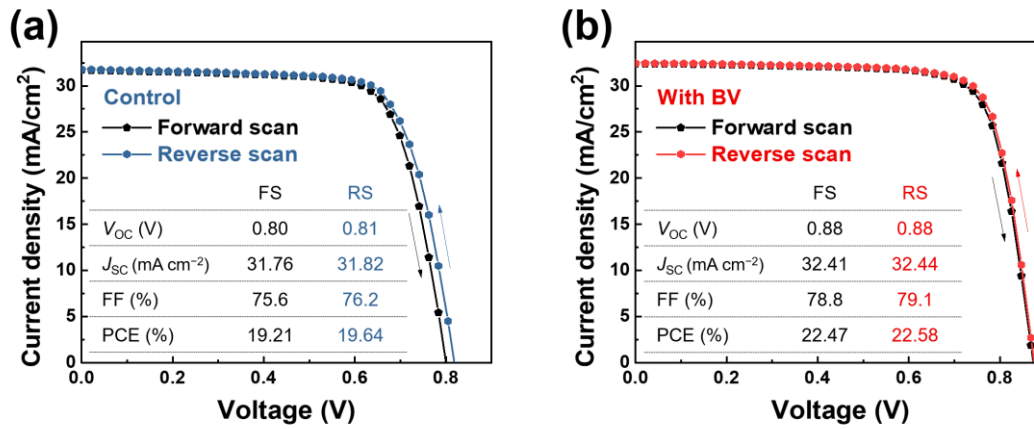
Figure S9. The photocurrent density-voltage (*J-V*) measurement curves of the PSCs in both forward and reverse scan directions.
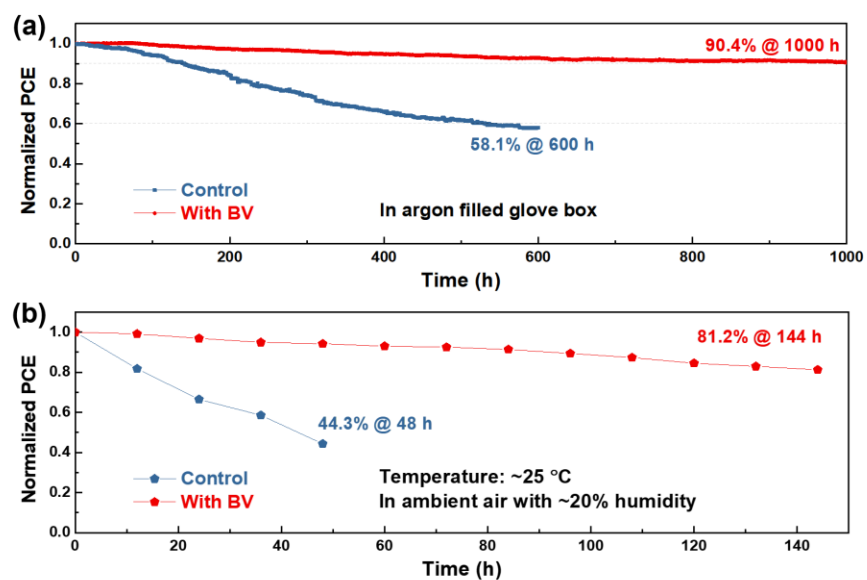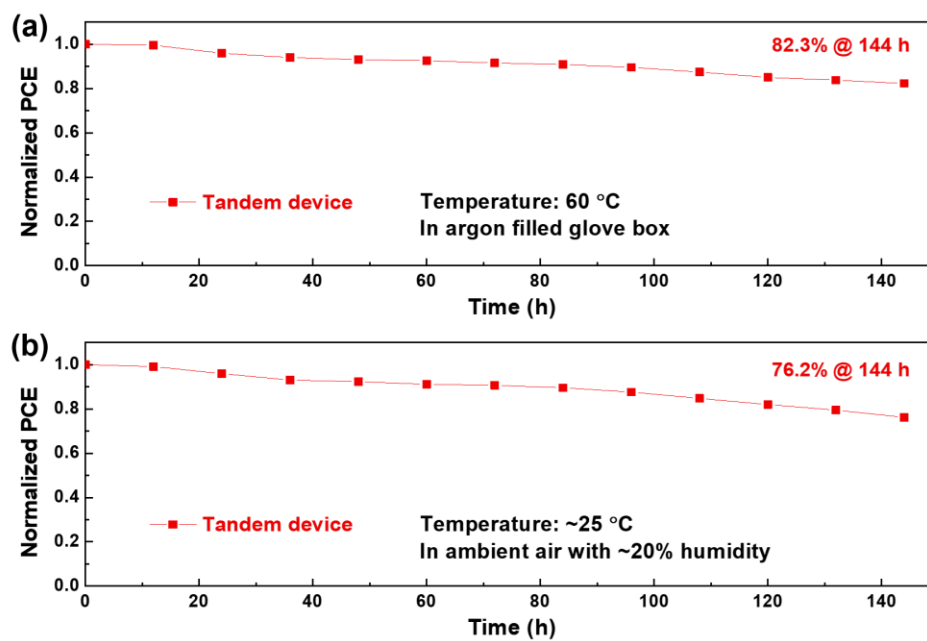
Figure S10. (a) Operational stability test of the control and the BV-treated PSCs monitored at the maximum power point in argon-filled glovebox. (b) Stability test of the control and the BV-treated PSCs in ambient air with ~20% relative humidity.

Figure S11. (a) Cross-sectional SEM image of the wide-bandgap $FA_{0.8}Cs_{0.2}PbI_{1.8}Br_{1.2}$ device. (b) The photocurrent density-voltage measurement curves of the optimized wide-bandgap PSC. (c) The stabilized power output of the optimized wide-bandgap PSC at the maximum power point voltage. (d) The EQE curves of the optimized wide-bandgap PSC.

The wide-bandgap PSCs were fabricated with a planar heterojunction configuration of ITO/PTAA/perovskite/C_{60}/BCP/Ag. Figure S11a presents the cross-sectional SEM image of a completed wide-bandgap device, from which about 350 thick, highly crystalline perovskite film can be observed. The optimized device achieved a PCE of 17.83%, with a V_{OC} of 1.25 V, a J_{SC} of 17.87 mA cm^{-2}, and a FF of 79.8% in reverse scan direction (Figure S11b). The stabilized output PCE of the device was measured to be 17.63% with a stabilized J_{SC} of 16.63 mA cm^{-2} (Figure S11c). Figure S11d presents the external quantum efficiency (EQE) curves (left coordinate) of the optimized device. The integrated current density (right coordinate) obtained from the EQE curve was calculated to be 17.22 mA cm^{-2}, very close to the measured values of J_{SC}.

Figure S12. (a) Stability test of the optimized tandem cell measured under 60 °C aging condition in argon-filled glovebox. (b) Stability test of the optimized tandem cell measured in ambient air with ~20% relative humidity.

Table S1. Fitting parameters of PL decay lifetime of the control and the BV-treated Sn-Pb perovskite films with different thicknesses deposited on glass substrate.

		τ_1 (ns)	A_1	τ_2 (ns)	A_2	τ_{ave} (ns)
Control	1000 nm	22.30	0.83	90.89	0.17	33.96 ns
	760 nm	17.32	0.84	82.63	0.16	27.77 ns
	550 nm	11.35	0.81	64.6	0.19	21.47 ns
	360 nm	7.37	0.79	41.04	0.21	14.43 ns
	220 nm	5.43	0.84	30.12	0.16	9.38 ns
With BV	1000 nm	51.97	0.67	361.85	0.33	154.23 ns
	760 nm	42.69	0.71	255.74	0.29	104.47 ns
	550 nm	17.06	0.70	156.18	0.30	58.80 ns
	360 nm	12.79	0.76	84.30	0.24	29.95 ns
	220 nm	9.04	0.79	53.83	0.21	18.45 ns

Table S2. Photovoltaic parameters of the devices.

		V_{OC} (V)	J_{SC} (mA cm^{-2})	FF (%)	PCE (%)
Control	Reverse	0.81	31.82	76.2	19.64
	Forward	0.80	31.76	75.6	19.21
With BV	Reverse	0.88	32.44	79.1	22.58
	Forward	0.88	32.41	78.8	22.47
2-T tandem	Reverse	2.12	15.78	78.7	26.33
	Forward	2.10	15.74	78.5	25.95

Reference:

1. D. Kiriya, M. Tosun, P. Zhao, J. Kang, A. Javey. *J. Am. Chem. Soc.* 2014, *136*, 7853-7856.

2. E. Gaulding, J. Hao, H. Kang, E. Miller, S. Habisreutinger, Q. Zhao, A. Hazarika, P. Sercel, J. Luther, J. Blackburn. *Adv. Mater.* 2019, *31*, 1902250.

3. Y. Zhou, C. Fei, M. Uddin, L. Zhao, Z. Ni, J. Huang. *Nature* 2023, *616*, 712-718.

4. X. Liu, M. Xu, Y. Hao, J. Fu, F. Wang, B. Zhang, S. Bennett, P. Sellin, W. Jie, Y. Xu. *ACS Appl. Mater. Interfaces* 2021, *13*, 15383-15390.

5. Y. Hu, A. Ruud, V. Miikkulainen, T. Norby, O. Nilsen, H. Fjellvag. *RSC Adv.* 2016, *6*, 60479-60486.